

# Fusion Welding of Glass Using Femtosecond Laser Pulses with High-repetition Rates

Isamu MIYAMOTO\*, Alexander HORN\*\*, Jens GOTTMANN\*\*,  
Dirk WORTMANN\*\*, Fumiyo YOSHINO\*\*\*

\*Osaka University, 2-1 Yamada-Oka, Suita, Osaka 565-0871, Japan

E-mail: isamu.miyamoto@areseonet.ne.jp

\*\* Lehrstuhl für Lasertechnik, RWTH-Aachen, Steinbachstrasse 15, 52074 Aachen, Germany

\*\*\* Applications Research Laboratory, IMRA America, Inc. Fremont, CA 94538 USA

Laser energy of femtosecond pulses absorbed by the nonlinear process is utilized as a heat source for fusion welding of glass. A femtosecond fiber laser, IMRA America, FCPA  $\mu$ Jewel D-4001, with variable repetition rates between 100kHz and 5MHz, was focused with a lens of NA0.65 into borosilicate glass (Schott D263) at different pulse energies, repetition rates and traveling velocities for local melting. The temperature distribution was calculated using a thermal conduction model where instantaneous heat is periodically deposited in a moving rectangular solid. The nonlinear absorptivity of the femtosecond laser pulses increased significantly as the repetition rate increased by the contribution of avalanche ionization caused by the increase in temperature at the laser-irradiation region. The calculated values agreed well with the experimental melt dimensions in a velocity range of 0.5~200mm/s, when the experimental values of the nonlinear absorptivity and the dimensions of the nonlinear absorption region were used for temperature calculation. The fusion welding of glass by femtosecond laser provided much higher melting and joining efficiencies than existing laser welding of metals.

**Keywords:** Femtosecond laser pulse, nonlinear absorption, thermal conduction, welding, melting, internal modification, glass

## 1. Introduction

Glass has a lot of potential applications in optics, MEMS, electronics, and biomedical due to its excellent optical, mechanical, electrical and chemical properties. The disadvantage is, however, that reliable joining techniques for glass are not available, and thus the glass joining has relied on the techniques based on adhesive agent or interlayer, which causes poor mechanical, thermal and chemical durability.

In recent years, femtosecond laser pulses have been used for a variety of internal modifications of transparent materials including direct writing of optical waveguides [1,2], three-dimensional binary data storage [3], and writing of optical amplifiers [4]. Welding of fused silica was also reported using femtosecond laser pulses [5], but the welding speed was as low as 5 $\mu$ m/s due to the low repetition rate of the laser used. Recently femtosecond lasers at high-repetition rates with reasonably high pulse energies became commercially available, enabling modified area much larger than the focused volume [6,7]. The enlarged modification region was attributed to the heat accumulation based on the numerical calculation of the temperature distribution using a thermal conduction models where the stationary heat source with spherical or spherical Gaussian distribution was assumed [7,8]. They are too simple, however, to estimate the modified dimensions in the waveguide writing as well as fusion welding, since the laser beam is

actually deposited in the area elongated along the optical axis of the laser beam, and moves at a constant velocity.

In this paper, local melting of glass by femtosecond laser pulses is reported, and the spatial and temporal distributions of the temperature are calculated by a thermal conduction model [9] where the heat is generated in a moving rectangular solid with the size of the focus diameter and the length of the nonlinear absorption along the optical axis. The interaction between bulk glass and fs laser pulse is also discussed based on the absorption data, the modified features and the thermal conduction analysis.

## 2. Experimental procedures

An amplified Yb-fiber laser with 406fs at 1MHz and 325fs at 100kHz pulses at 1045nm with a beam quality of  $M^2 < 1.5$  was focused by an aspheric lens with NA0.65, providing diffraction-limited focusing of approximately 2 $\mu$ m  $1/e^2$  in diameter. The laser beam was focused into the glass sample moving linearly at velocities between 0.5 and 200mm/s using computer-controlled motion stages.

**Table 1 Thermal properties of Schott D263 [10]**

Properties	Values
Density $\rho$ (g/cm <sup>3</sup> )	2.51
Specific heat $c$ (J/gK) <sup>1)</sup>	0.82
Thermal conductivity $K$ (J/s.cm.K) <sup>2)</sup>	0.0096
Thermal diffusivity $\alpha=K/c\rho$ (cm <sup>2</sup> /s)	0.0046
Melting temperature $\theta_m$ (°C) <sup>3)</sup>	1051

<sup>1)</sup>mean value 20~100°C, <sup>2)</sup>value of Corning 0211, <sup>3)</sup>forming temperature

As the specimen, borosilicate glass, Schott D263, with thicknesses of 1mm and 0.2 mm was used, of which thermal properties are shown in **Table 1**.

The time-averaged laser power passing through the specimen was measured by a power meter to determine the laser power deposited in the glass specimen by the nonlinear absorption, as shown in **Fig. 1**. Since the glass specimen used is transparent to the laser wavelength, the absorption is considered to be due to the nonlinear process. Neglecting the scattering and the reflection of the laser beam at the focus, the nonlinear absorptivity of the laser beam  $A$  is given by

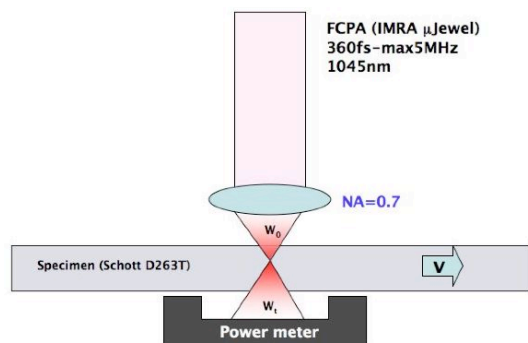


**Fig.1** Schematic illustration experimental set up. Averaged laser power passing through the glass sample was measured to determine the nonlinear absorptivity.

$$A = 1 - \frac{W_t}{W_0} \frac{1}{(1-R)^2} \quad (1)$$

where  $W_0$  is the incident laser power to the work piece,  $W_t$  the transmitted laser power and  $R$  the reflectivity of the laser beam at the glass surface. Laser-irradiated specimens were observed by an optical microscope.

### 3. Results and discussions

#### 3.1 Melting characteristics

Ultrashort laser pulses with femtosecond duration were focused into borosilicate glass (Schott D263) at different traveling velocities. **Figure 2** shows the cross sections of the laser-irradiated specimen made at a pulse repetition rate of 1MHz at 0.5μJ per pulse, and a 100kHz at 2.2μJ per pulse.

No cracks are seen in the modified region and the surrounding area in **Fig. 2**. This is rather surprising from the common sense that cracks are normally developed in local melting of glass with pulse duration longer than ns except for glass having low thermal expansion coefficient like fused silica [11]. This is because the tensile stress in local melting of brittle material exceeds the material strength during heating period in the surrounding area of the heating spot or during cooling period in the melted region by the shrinkage of the melted region [12]. Stress wave can also cause cracks in fused silica, since it propagates faster than thermal diffusion [13]. There are, however, some possibilities to suppress the crack propagation. The propagation of the cracks with very small size can be suppressed, because the stress intensity factor is proportional to the square root

of the cracks [14]. The other possibility to suppress the cracking is the contribution of the ballistic electrons; the electrons produced in the nonlinear absorption process can reach very high velocities to suppress the cracking by changing the surrounding area from brittle to ductile condition, since they move much faster than the stress wave. There is, however, a puzzling phenomenon reported by Vanagas *et al.* [15], where crack-free melting was realized utilizing the two-photon absorption with 12ns-laser pulse at 355nm for 3D recording application in borosilicate glass. Further study is needed to understand the mechanisms of the crack propagation and suppression in glass melting by ultrashort laser pulses.

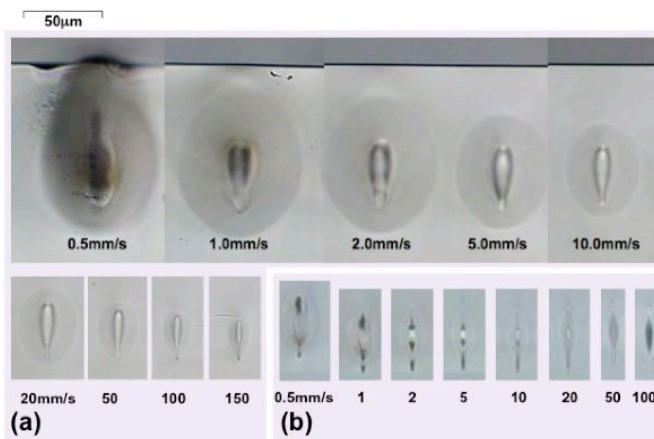


**Fig.2** Cross sections of laser-irradiated borosilicate glass (Schott D263) with femtosecond pulses at different traveling velocities at (a) 1MHz-0.5μJ and (b) 100kHz-2.2μJ.

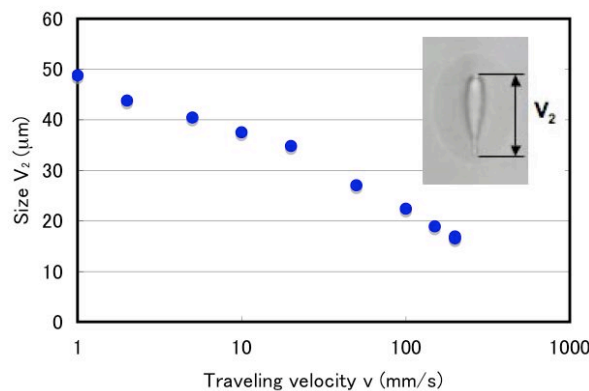


**Fig.3** Vertical size of the inner region  $V_2$  vs. traveling velocity at 1MHz at 0.5μJ.

The modified region consists of the inner region with teardrop-shape extended along the optical axis and the surrounding outer elliptical region. At 1MHz, the shape of the inner region is similar to that of the modified region produced by the irradiation of single laser pulses [16], indicating that the inner region is produced by the direct effect of the laser pulse to provide high temperature and high pressure [17]. In the outer region, the glass is heated by the conduction of the heat transferred from the laser-excited electrons to the lattice, so that the outer region expands to the area much larger than the size of focused volume. The outer region is heated above the melting temperature of the glass to enable fusion welding [9,18]. The pressure of the

inner region is sustained by the solid glass. It is seen, however, that when the melt region reaches the surface of the specimen at  $0.5\text{mm/s}$ , the interface between the inner and outer regions is broken at the top edge by the pressure of the inner region, so that the pressurized hot melt is ejected into the outer region.

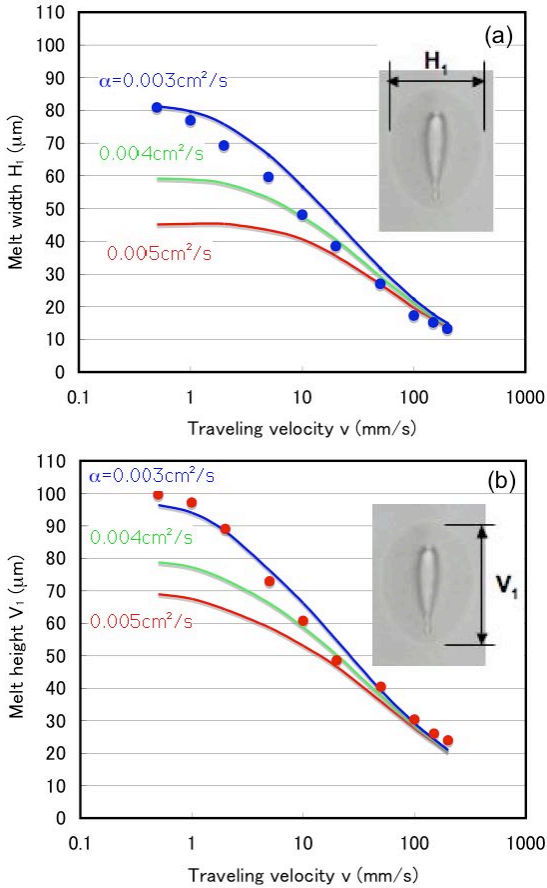


**Fig.4** Calculated and experimental melt width  $H_1$  and height  $V_1$  plotted as a function of traveling velocity at  $1\text{MHz}-0.5\mu\text{J}$  for different values of thermal diffusivity  $\alpha$  for Schott D263.

**Figure 3** shows the vertical length  $V_2$  of the inner region plotted vs. traveling velocity. The value  $V_2$  decreases exponentially with increasing the traveling velocity. The horizontal and vertical sizes of the outer region,  $H_1$  and  $V_1$ , are plotted in **Fig. 4**.

It is noted that the cross-sectional area of the outer regions in  $100\text{kHz}$  is much smaller than in  $1\text{MHz}$  even taking into consideration of 2.3 times difference in the average laser power; at  $0.5\text{mm/s}$ , for instance, the cross-sectional area of the outer region in the  $100\text{kHz}$  is 7~8 times smaller than that in the  $1\text{MHz}$ . This is attributed to the lower non-linear absorptivity of the laser energy at lower pulse repetition rate as described below.

### 3.2 Thermal conduction model

A thermal conduction model was developed to calculate the transient temperature distributions in fusion welding by ultrashort laser pulses where instantaneous heat pulse are delivered periodically in a rectangular solid moving at a constant velocity  $v$  in an infinite solid [9]. In this

model, an analytical equation was derived by a spatial and temporal integration of the solution of the instantaneous point heat source in an infinite solid with zero temperature [19], assuming that the thermal properties are independent of the temperature.

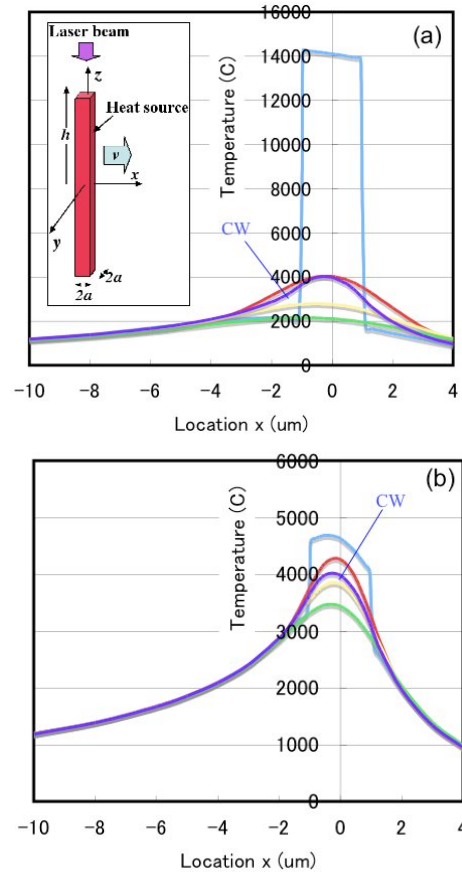


**Fig.5** Transient temperature distributions along  $x$ -axis ( $y=z=0$ ) at different time  $t$  after the latest pulse irradiation calculated by Eq(2) ( $v=100\text{mm/s}$ , average power= $200\text{mW}$ ,  $a=1\mu\text{m}$ ,  $h=10\mu\text{m}$ ). Light blue:  $t=0$ , red:  $t=0.3T$ , yellow:  $t=0.6T$  and green:  $t=0.999T$ . (a)  $100\text{kHz}-2\mu\text{J}$ , (b)  $1\text{MHz}-0.2\mu\text{J}$

Assuming that the latest laser pulse is irradiated when the center of the rectangular solid moving at a velocity  $v$  along the  $x$ -axis ( $y=z=0$ ) locates at the origin of the coordinate at time  $t=0$ , as shown in the inset of **Fig. 5**, the temperature rise  $\theta$  at time  $t$  at location  $(x,y,z)$  in quasi steady state is given by

$$\theta(\xi,\psi,\zeta;\tau) = \frac{AQ}{64c\rho r} \sum_{i=0}^{\infty} \left( \operatorname{erfc} \frac{\xi + i v \Xi^2 / 2 - \delta}{\tau \sqrt{(i \Xi^2 / \tau^2 + 1)}} - \operatorname{erfc} \frac{\xi + i v \Xi^2 / 2 + \delta}{\tau \sqrt{(i \Xi^2 / \tau^2 + 1)}} \right) \cdot \left( \operatorname{erfc} \frac{\psi - \delta}{\tau \sqrt{(i \Xi^2 / \tau^2 + 1)}} - \operatorname{erfc} \frac{\psi + \delta}{\tau \sqrt{(i \Xi^2 / \tau^2 + 1)}} \right) \cdot \left( \operatorname{erfc} \frac{\zeta - \eta}{\tau \sqrt{(i \Xi^2 / \tau^2 + 1)}} - \operatorname{erfc} \frac{\zeta + \eta}{\tau \sqrt{(i \Xi^2 / \tau^2 + 1)}} \right) \quad (2)$$

$$\text{where } \operatorname{erfc} U = \frac{2}{\sqrt{\pi}} \int_U^{\infty} \exp(-u^2) du.$$

Here  $Q$  is pulse energy,  $A$  nonlinear absorptivity,  $f$  repetition rate of laser pulse ( $T=1/f$ ),  $2a$  focus diameter of the laser beam,  $2h$  length of the rectangular solid,  $c$  the specific heat of the material and  $\rho$  density of the material. In this

equation, the following non-dimensional parameters are used ( $r^3=a^2h$ ).

$$\xi = \frac{x}{r}, \quad \psi = \frac{y}{r}, \quad \zeta = \frac{z}{r}; \quad \delta = \frac{a}{r} = n^{-1/3}, \quad \eta = \frac{h}{r} = n^{2/3},$$

$$\tau = \frac{1}{r} \sqrt{4\alpha t}, \quad \Xi = \frac{1}{r} \sqrt{4\alpha T}, \quad \text{and} \quad v = \frac{vr}{2\alpha} \quad (3)$$

Figure 5 shows the quasi-steady temperature distributions calculated along the  $x$ -axis at different time after the laser pulse irradiation, assuming that an average laser power of  $0.2W$  ( $1MHz-0.2\mu J$  and  $100kHz-2\mu J$ ) is deposited in the glass. At  $100kHz-2\mu J$ , the temperature just before the pulse arrival (green line) is much lower than that at  $1MHz-0.2\mu J$  due to longer cooling time, although the temperature at the moment of the pulse arrival is much higher due to its higher pulse energy.

The steady temperature distribution due to CW (continuous wave) heat source model [9] was also calculated, where continuous laser power of  $W=fQ$  is delivered uniformly in the rectangular solid, and is given by

$$\Theta(\xi, \psi, \zeta) = \int_0^\infty \left\{ \operatorname{erfc}\left(\frac{\xi-\delta}{\tau} + \frac{v\tau}{2}\right) - \operatorname{erfc}\left(\frac{\xi+\delta}{\tau} + \frac{v\tau}{2}\right) \right\} \cdot \left( \operatorname{erfc}\frac{\psi-\delta}{\tau} - \operatorname{erfc}\frac{\psi+\delta}{\tau} \right) \left( \operatorname{erfc}\frac{\zeta-\delta}{\tau} - \operatorname{erfc}\frac{\zeta+\delta}{\tau} \right) \tau \cdot d\tau$$

$$\text{where } \theta(x, y, z) = \frac{AQf}{128Kr} \Theta(\xi, \psi, \zeta).$$

In Fig. 5, temperature distribution due to CW model is also plotted in a blue line. It is seen that the temperature rise due to the pulsed model can be approximated by CW model at locations several  $\mu m$  apart from the heat source. Thus the molten sizes are estimated using the simpler equation given by Eq(4) in the following section.

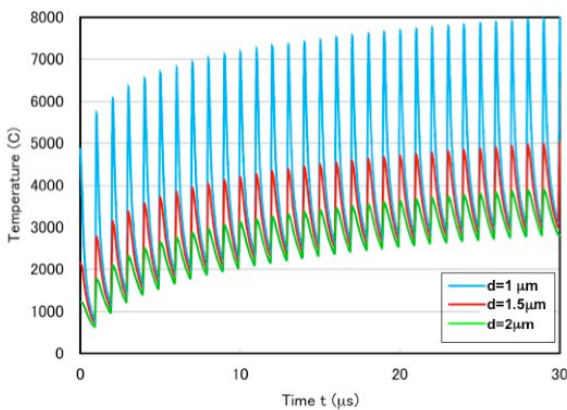


Fig.6 Temperature change calculated at the center of stationary rectangular solid with heat source sizes of  $d=1$ ,  $d=1.5$  and  $d=2\mu m$  ( $1MHz-0.5\mu J$ ,  $2h=20\mu m$ ).

As seen in Fig. 5(a), the temperature distribution is flat-top at time  $t=0$  reflecting of the uniform intensity in the rectangular solid. However, the peak temperature at the heat source center calculated by the model is accurate, if the uniform intensity is equal to the center of the heat source for any distributions, since the heat is liberated instantaneously. It should be also noted that the temperature distribution depends not only on the distribution but also on the size of the heat source, which are

the size of the heat source, which are difficult to know exactly due to many effects including the refractive index distribution, the aberration, the self-focusing and so on. So the temperature change was calculated at different values of  $d$  using Eq(2). Figure 6 shows the temperature change calculated at the center of the heat source for different values of  $d$ . Little dependence of the minimum temperature is seen on  $d$ , although the maximum temperature rise per pulse is proportional to  $1/d^2$ . This means that the model provides the accurate temperature at the moment just before the incidence of the laser pulse, even if the estimation of the focus spot size has some error.

### 3.3 Melting characteristics of glass with femtosecond laser pulses

The temperature distributions corresponding to Fig. 2(a) were calculated using Eq(4). For the calculation, it is necessary to determine the dimensions of the rectangular solid ( $a$  and  $h$ ) and the nonlinear absorptivity  $A$ . As the value of  $2a$ , the focus diameter of  $2\mu m$  was used. It was assumed  $2h$  is equal to be  $\gamma \times V_2$  ( $\gamma < 1$ ) instead of  $V_2$ , to take the effect of the thermal conduction into consideration to some extent. In this study, we adopted  $\gamma=0.9$  arbitrarily. As to the absorptivity, the experimental values measured from Eq(1) were used, which will be shown in Fig. 8.

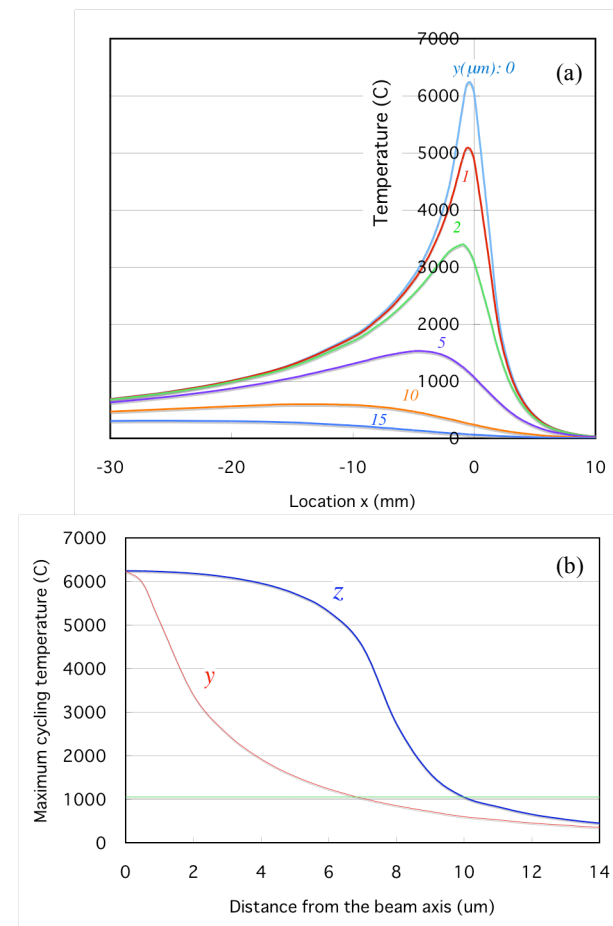
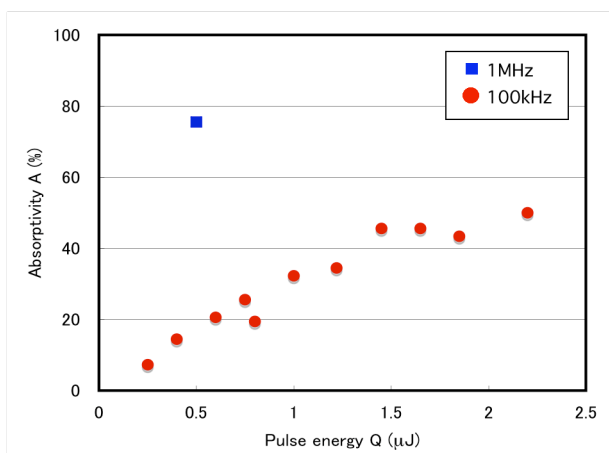


Fig.7 Temperature distribution calculated for  $1MHz-0.5\mu J$  ( $v=200\text{ mm/s}$ ,  $a=1\mu m$ ,  $h=15.5\mu m$ ). The absorptivity of 0.6 extrapolated in Fig.8 is used. (a) Steady temperature along the  $x$ -axis for different  $y$  ( $z=0$ ). (b) Maximum temperature distribution along  $y$ - and  $z$ -axes.

**Figure 7(a)** shows the steady temperature distributions calculated along the  $x$ -axis at different values of  $y$  at  $z=0$  at a traveling velocity  $200\text{mm/s}$  at  $1\text{MHz}-0.5\mu\text{J}$ . Each curve shows a temperature cycle, of which maximum cycle temperature is reached behind the heat source. **Figure 7(b)** shows the distributions of the maximum cycle temperature in the  $xy$ - and the  $xz$ -planes. One can find the horizontal and vertical melt dimensions,  $H_l$  and  $V_l$ , from the melting temperature of the glass,  $\theta_m=1051^\circ\text{C}$ .

The melt dimensions of  $H_l$  and  $V_l$  thus calculated are plotted as a function of the traveling velocity at  $1\text{MHz}-0.5\mu\text{J}$  in **Fig. 4**. At higher traveling velocities, the calculated values of  $H_l$  and  $V_l$  agree well with the experimental values with the thermal diffusivity  $\alpha=0.005\text{cm}^2/\text{s}$ , which is nearly equal to the value at room temperature,  $\alpha=K/c\rho=0.0046\text{cm}^2/\text{s}$  using  $K=0.009\text{J/s.cm.K}$  given in **Table 1**. As the traveling velocity decreases, however, the calculated melt dimensions tend to saturate at  $v<5\text{mm/s}$ , whereas the experimental values still continue to increase. Thus the calculated values agree with the experimental values with lower thermal diffusivities of  $\alpha=0.004\text{cm}^2/\text{s}$  at around  $10\text{mm/s}$ , and  $\alpha=0.003\text{cm}^2/\text{s}$  around  $1\text{mm/s}$ . This is thought to be because the effective thermal diffusivity decreases with increasing temperature.



**Fig.8** Nonlinear absorptivity of Schott D263 determined as a function of pulse energy  $Q$ .

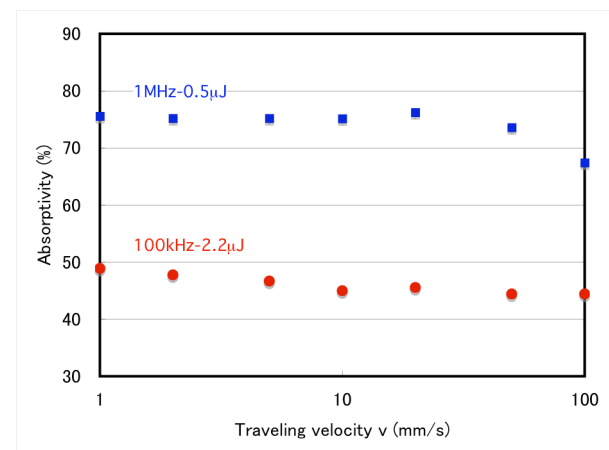


**Fig.9** Nonlinear absorptivity of Schott D263 determined as function of traveling velocity  $v$ .

### 3.4 Characteristics of nonlinear absorptivity

The nonlinear absorptivity vs. pulse energy at  $100\text{kHz}$  with static exposure ( $v=0$ ) is shown in **Fig. 8**. The absorptivity increases with increasing pulse energy due to the increased photoionization rate [20].

The nonlinear absorptivity at  $1\text{MHz}-0.5\mu\text{J}$  determined at  $v<20\text{mm/s}$  is also plotted in the figure, and was approximately 4 times higher than that at  $100\text{kHz}$  at  $0.5\mu\text{J}$ , indicating that the nonlinear absorptivity is strongly influenced by the pulse repetition rate in sub-picosecond duration. The temperature at the laser-irradiating region just before the pulse arrival ( $t=0.999T$ ),  $\theta_B$ , at  $Q=0.5\mu\text{J}$  was calculated at  $1\text{MHz}$  and  $100\text{kHz}$ . The temperature  $\theta_B$  at  $1\text{MHz}$  was approximately  $8500^\circ\text{C}$ , whereas  $\theta_B$  at  $100\text{kHz}$  was approximately as low as  $100^\circ\text{C}$ . This indicates that the higher nonlinear absorptivity at  $1\text{MHz}$  is caused by the larger number of the thermally excited electrons in the conduction band from the valence band.

The absorptivity measured at  $100\text{kHz}-2.2\mu\text{J}$  and  $1\text{MHz}-0.5\mu\text{J}$  is plotted vs. traveling velocity in **Fig. 9**, corresponding to **Fig. 2**. The absorptivity at  $1\text{MHz}$  is higher than  $100\text{kHz}$  again in spite that the pulse energy of  $1\text{MHz}$  is approximately 4 times less than  $100\text{kHz}$ .

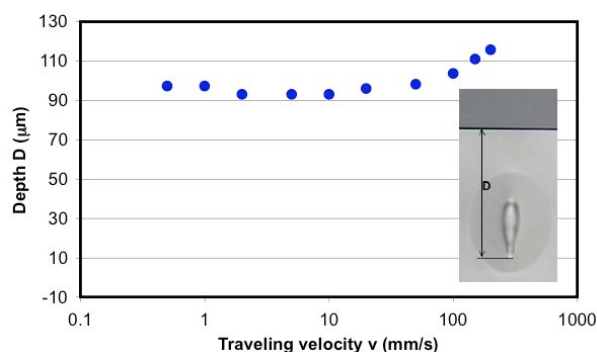


**Fig.10** Depth of the tip of the teardrop-shaped inner region  $D$  measured as a function of traveling velocity at  $1\text{MHz}-0.5\mu\text{J}$ .

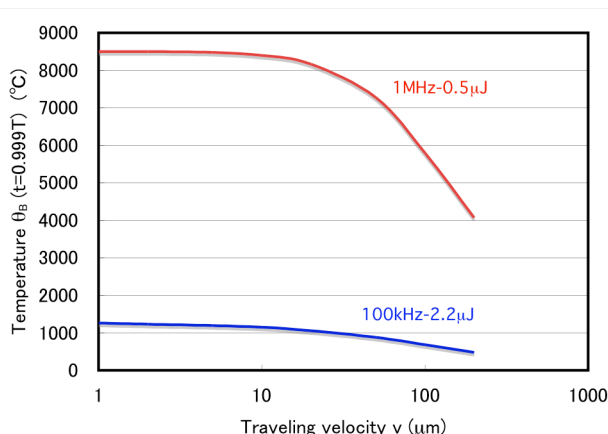


**Fig.11** Temperature  $\theta_B$  calculated at the center of the rectangular solid heat source at time  $t=0.999T$  vs. traveling velocity. Cross sections are shown in **Fig. 2**.

The depth of the tip of the teardrop  $D$  was measured from the surface at different traveling velocities. Special attention was paid to keep the focal position constant from

the surface. Only the depth  $D$  of  $1\text{MHz}-0.5\mu\text{J}$  is plotted vs. traveling velocity in Fig. 10, since the melt patterns of  $100\text{kHz}-2.2\mu\text{J}$  were not so clear to measure  $D$  precisely. Although  $D$  was almost constant at velocities  $v < 20\text{mm/s}$ , it began to increase at velocities faster than  $20\text{mm/s}$  in accordance with the decrease in the absorptivity shown in Fig. 9.

In order to understand the process, the temperature at the center of the laser irradiation zone just before the pulse arrival ( $t=0.9999T$ ),  $\theta_B$ , was calculated as a function of traveling velocity. Figure 11 shows thus calculated temperature  $\theta_B$  for  $100\text{kHz}-2.2\mu\text{J}$  and  $1\text{MHz}-0.5\mu\text{J}$  where measured absorptivity and heat source size were used. The temperatures  $\theta_B$  at  $1\text{MHz}-0.5\mu\text{J}$  in a range  $v < 20\text{mm/s}$  was as high as  $\theta_B = 8500^\circ\text{C}$ , which provides approximately 0.4% of electrons thermally excited to the conduction band, assuming that the band gap of the material is  $4\text{eV}$ . It is also expected to increase the seed electrons from the impurity and defect states. On the other hand,  $100\text{kHz}-2.2\mu\text{J}$  resulted in  $\theta_B = 1200^\circ\text{C}$ , of which the number of the thermally excited electrons are negligible. Thus the seed electrons for avalanche ionization during the rest of the laser pulse depend solely on photoionization in the leading edge of the pulse [20,21]. Our results indicate that thermally excited electrons from the valence band to the conduction band can play an important role in increasing the number of the seed electrons for the avalanche ionization in sub-picosecond pulses at higher repetition rates.

We found that three independent results, the nonlinear absorptivity, the depth of the teardrop tip, the temperature, closely link together as mentioned above. The effect of the pulse repetition rate on the nonlinear absorption can be interpreted as follows.

The nonlinear absorption starts at the tip of the teardrop when the leading edge of the laser pulse has energy corresponding to the intensity threshold for the breakdown at the location upstream of the laser focus. Increase in the repetition rate increases the nonlinear absorptivity due to increased thermally excited electrons in conduction band. When the number of the thermally excited electrons decreases at higher traveling velocities, higher laser intensity is required for breakdown, so that the starting point of the breakdown approaches to the focus point having higher laser intensity. The shape of the teardrop is considered to be the result of different temporal slices of the energy above the threshold. Subsequent time slices of the pulse have energy to produce breakdown upstream from the tip, and breakdown proceeds further upstream having larger laser beam diameter, leading to the formation of the teardrop. In this discussion, the effect of the refractive index change was neglected.

It has been reported that the melt dimensions in  $1\text{MHz}$  is much larger than those in  $100\text{kHz}$  in borosilicate glass with  $\text{fs}$  second pulses, and this was accounted for by the increased heat accumulation at higher pulse repetition rates [7]. The present study showed that the increase in the melt dimensions at  $1\text{MHz}$  is caused not only by the heat accumulation, but also by the increase in the nonlinear absorptivity due to the increased number of the thermally excited electrons to the conduction band.

### 3.5 Welding performance with ultrashort laser pulses

Welding performance of glass using ultrashort pulse lasers was estimated by the melting efficiency  $\eta$  and the joining efficiency  $R$ . The melting efficiency  $\eta$  [22] is defined by the ratio of the power required for elevating the temperature of the volume of the weld bead up to the melting temperature  $\theta_m$  to the incident laser power  $W_0$ , and is given by

$$\eta = \frac{Sv\rho\theta_m}{W_0} \tag{8}$$

where  $S$  is the cross sectional area given by  $\pi H_1 V_1 / 4$ . As is seen in Fig.11(a),  $\eta$  increases with increasing traveling velocity, reaching approximately 22% at  $100\text{mm/s}$ .

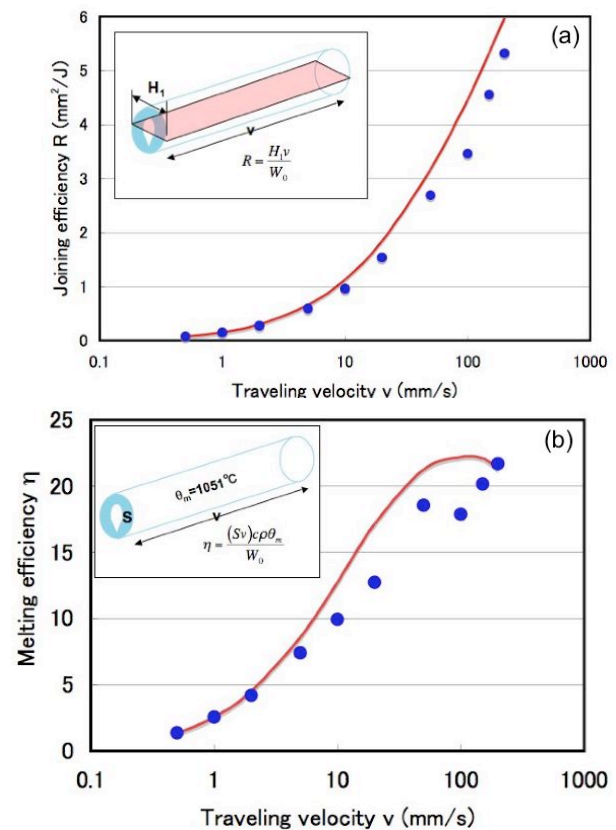


Fig.12 Efficiencies estimated in glass welding of Schott D263 at  $1\text{MHz}-0.5\mu\text{J}$ . Cross sections are shown in Fig. 2(a). (a)Melting efficiency, (b) joining efficiency

The joining efficiency  $R$  [22] is defined by the joint area at the interface per unit laser energy, and is given by

$$R = \frac{H_1 v}{W_0} \tag{9}$$

The joining efficiency increases with increasing traveling velocity, and reaches as high as  $5.3\text{mm}^2/\text{J}$ , as shown in Fig. 11(b). It should be noted that this value is much larger than the largest value attained in the past in metal welding,  $2.5\text{mm}^2/\text{J}$ , which was obtained by single-mode fiber laser [23,24], indicating that the fusion welding of glass by femtosecond laser pulses is extremely efficient. This is because laser energy is delivered instantaneously to the glass by the nonlinear process. Higher efficiency is expected at higher welding velocities using higher average power.

#### 4. Conclusions

Femtosecond laser pulses were used as a heat source for local melting glass and applied to fusion welding of glass plates. The welding process was discussed based on the thermal conduction model developed to calculate the spatial and temporal distribution of temperature where ultrashort laser pulses are deposited periodically into a moving rectangular solid, determined by the nonlinear absorption process. The model provides useful information for optimization of ultrafast laser processing such as fusion welding and optical waveguide writing. The results obtained in this study is summarize as follows:

- (1) Femtosecond lasers with high pulse-repetition rates provide an efficient fusion welding, which melts selectively the joining interface at welding speeds faster than  $100\text{mm/s}$ .
- (2) The molten dimensions calculated by the thermal conduction model agree well with the experimental melt size taking into consideration that the thermal diffusivity decreases with increasing the temperature.
- (3) The nonlinear absorptivity of the femtosecond laser pulses is strongly affected by the repetition rate of the laser pulses. This is because the temperature just before the pulse arrival increases with increasing the repetition rate so that the contribution of thermally excited electrons to conduction band increases to enhance the avalanche ionization.
- (4) Fusion welding of glass by femtosecond laser pulses provides extremely high joining efficiency, which has never attained in fusion welding of metal.

#### References

- [1] K. Miura, J. R. Qiu, H. Inoue, T. Mitsuyu, K. Hirao, Appl. Phys. Lett. **71**, p. 3329 (1999)
- [2] M. Will, S. Nolte, B. N. Chichkov, A. Tunnermann: Appl. Optics, **41**, p. 4360 (2002)
- [3] M. Watanabe, H. B. Sun, S. Juodkazis, T. Takahashi, S. Matsuo, Y. Suzuki, J. Nishii, H. Misawa: Jpn. J. Appl. Phys., Part 2, **37**, p. 1527 (1998)
- [4] Y. Sikorski, A. A. Said, P. Bado, R. Maynard, C. Florea, K. A. Winick: Electron. Lett, **36**, p. 226 (2000)
- [5] T. Tamaki, W. Watanabe, J. Nishii, K. Itho: Japanese J. Appl. Phys. **44**, p. L687 (2005)
- [6] S. Nolte, M. Will, J. Burghoff, A. Tunnermann: J. Modern Optics **10**, p. 2533 (2004)
- [7] S. M. Eaton, H. Zhang, P. Herman, F. Yoshino, L. Shah, J. Bovatsek, A. Y. Arai: Optics Express, **13**, p. 4708 (2005)
- [8] C. B. Schaffer, J. F. Garcia, E. Mazur: Appl. Phys. A, **76**, p.351 (2003)
- [9] I. Miyamoto, A. Horn, J. Gottmann: Proc. LAMP2006 (2006) to be published
- [10] Private communication with Dr. Hermanns, Schott Glass
- [11] Y. Arata, H. Maruo, I. Miyamoto, S. Takeuchi: Proc. 7<sup>th</sup> International Conference on Electron and Ion Beam Science and Technology, p.111 (1976)
- [12] American Welding Society: Welding handbook, Vol. **1** (2001)
- [13] A. Horn, H. Khajehnouri, E.W. Kreutz, R. Poprawe, Proc. ICALEO'02, p.1577 (2002)
- [14] T. L. Anderson: Fracture Mechanics, CRC Press (1991)
- [15] E. Vanagas, J. -Y. Ye, M. Li, M. Miwa, S. Juodkazis, H. Misawa: Appl. Phys. **A81**, p. 725 (2005)
- [16] C. B. Schaffer, A. O. Jamison, E. Mazur: Appl. Phys. Lett., **84**, p. 1441 (2004)
- [17] E. N. Glazer, E. Mazur: Appl. Phys. Lett., **71**, p. 882 (1997)
- [18] J. Bovatsek, A. Arai, C. B. Schaffer: Proc. CLEO'06 (2006) to be published
- [19] H. S. Carslaw, J. C. Jeager: Conduction of heat in solid, Oxford at the Clarendon Press, 2<sup>nd</sup> edition (1959)
- [20] B. C. Stuart, M. D. Feit, S. Herman, A. M. Rubenchik, B. W. Shore, M. D. Perry: Phys. Rev. **B53**, p. 1749 (1996)
- [21] C. B. Schaffer, A. Brodeur, E. Mazur: Meas. Sci. Technol. **12**, p. 1784 (2001)
- [22] A. A. Wells: Heat flow in welding, Welding Journal, p. 263s (1952)
- [23] G. Deadon: Proc. 3<sup>rd</sup> International WLT-Conference on Laser in Manufacturing, p. 615 (2005)
- [24] I. Miyamoto, S-J. Park, T. Ooie: Proc. ICALEO'02 , ISBN 0-912035-72-27 (2002)

(Received: July 11, 2006, Accepted: February 7, 2006)